Available online at www.sciencedirect.com
SCIENCE DIRECT
Polymer 46 (2005) 11330–11339
polymer
www.elsevier.com/locate/polymer

A depth-resolved look at the network development in alkyd coatings by confocal Raman microspectroscopy

Beáta Marton [a], Leo G.J. van der Ven [b], Cees Otto [c], Natallia Uzunbajakava [c], Mark A. Hempenius [a], G. Julius Vancso [a,*]

[a] *Materials Science and Technology of Polymers, MESA+ Research Institute for Nanotechnology and Dutch Polymer Institute, University of Twente, P.O. Box 217, NL-7500 AE Enschede, The Netherlands*
[b] *Akzo Nobel Coatings Research Arnhem, P.O. Box 9300, NL-6800 SB Arnhem, The Netherlands*
[c] *Biomedical Technology Institute and MESA+ Research Institute, University of Twente, P.O. Box 217, NL-7500 AE Enschede, The Netherlands*

Received 26 October 2004; received in revised form 20 September 2005; accepted 4 October 2005
Available online 28 October 2005

Abstract

The formation of molecular networks related to the consumption of unsaturated carbon–carbon double bonds (C=C) during oxidative drying of alkyd coating films incorporating unsaturated fatty acids was studied. The concentration of C=C bonds was measured as a function of drying time and distance from the exposed film surface (depth) using confocal Raman microspectroscopy (CRM). The change in spatial distribution of the C=C double bond concentration across the film cross section provides information on the kinetics of the oxidative cross-linking process in the alkyd films. It was found that the C=C bond consumption is not homogeneous across the depth of the drying film. The results obtained allowed us to quantitatively monitor the progress of the drying process and the movement of the 'drying front' within the coating films. The drying profiles suggest that oxygen penetration into the coating film is a rate-limiting factor in the drying process. Depth profiles during the film forming process develop due to local variations in the oxygen solubility, diffusion coefficient of oxygen, and available amount of double bonds for cross-linking. The influence of several industrially relevant factors, like oil length of the alkyd resin, thickener, solvent, and drier on the film formation process is discussed. Depth resolution of the analytical approach and spatial accuracy of confocal Raman microspectroscopy are also treated.

Keywords: Alkyd paint; Cross-linking; Confocal Raman microspectroscopy, Depth profile of curing

1. Introduction

There is an increasing global demand for reducing the emission of volatile organic components (VOC) of paints and coatings due to the harmful effects that organic solvents, used in solvent-borne coatings, may have on the environment and paint users [1]. One of the options to reduce the emission of VOC is to replace organic solvents by water in coatings formulations. Alkyd resins, which form the basis of a very important class of coatings, can be transferred into water-borne systems using emulsification processes with the aid of surfactants [2]. Initially, water-borne coatings showed inferior performance when compared with solvent-borne systems. However, in view of recent advances in coatings technology, water-borne alkyds are becoming competitive with coatings made with organic solvents. Several application related properties like leveling out of brush or roller marks, open time, wet-edge time and filling capacity still need to be improved in order to make high gloss water-borne paints with equal—or better—performance than solvent-based products [3]. In aqueous coating systems, thickeners are used to provide adequate stability in storage and yield suitable rheological properties for applications [4,5].

Alkyds are oil-modified polyesters obtained by condensation reactions between polyhydric acids and polyhydric alcohols, and fatty acids from vegetable oils [1,6]. Depending on the oil content, the corresponding coatings show different properties [7]. After evaporation of the solvent, the alkyd film is very soft. The hardening of the alkyd paints is based on the cross-linking reaction of the fatty acid components, which occurs in the presence of oxygen in the film. The drying process consists of two main steps: oxidation of fatty acid chains and cross-linking between the chains. The film formation process is complicated; it involves a complex set of chemical processes occurring simultaneously as the fatty

* Corresponding author. Tel.: +31 534892967; fax: +31 534893823.
E-mail address: g.j.vancso@tnw.utwente.nl (G.J. Vancso).

0032-3861/$ - see front matter © 2005 Elsevier Ltd. All rights reserved.
doi:10.1016/j.polymer.2005.10.021

acid components undergo auto-oxidation reactions. Various strategies for chemical cross-linking of alkyds have been reviewed elsewhere [8,9]. The chemistry of the reactions involved can be efficiently studied using model compounds. Usually, methyl or ethyl esters of the unsaturated fatty acids are being used as model systems [10–13]. There is an important difference between the viscosity of oils and alkyds however, as the oil will be liquid like even after crosslinking. The changing viscosity as a function of time plays an important role in the drying process. The main steps of the chemical drying are summarized in Fig. 1.

Despite successes in application technologies, the scientific foundations of coatings often fall behind progress in applications. In view of the complexity of coatings systems and the relevant phenomena in polymer and surface science associated with film formation, scientific information available is often of qualitative, and observational nature. There is for example only little known about composition gradients in coatings films, and little information is available about the coating—substrate interphase. In order to better understand the film formation in water-borne alkyds, we used confocal Raman microspectroscopy (CRM) to monitor the chemical composition changes across the thickness of films as a function of time and depth from the film surface. The characterization of the film formation process requires spatially resolved and non-invasive techniques, which can probe the spatial uniformity of the reaction and the possibility of 'skin formation' at the surface. Only a few characterization techniques exist to fulfill these requirements. One of these is magnetic resonance imaging (MRI), where the changes in mobility of the polymer segments can be monitored as a function of spatial position (depth) [14,15]. Hyper frequency scanning acoustic microscopy is an alternative non-destructive microprobing technique, which is based on the measurement of Rayleigh wave velocity related to Young's moduli [16]. A non-direct way of determining the crosslink density changes in the depth of the film is possible by numerical modelling. A mathematical model was developed based on CRM and tensile measurements to predict the degree of effective cross-linking and the mechanical behavior of the drying coating films with different thickness [17] based on some assumptions regarding the modulus depth profile.

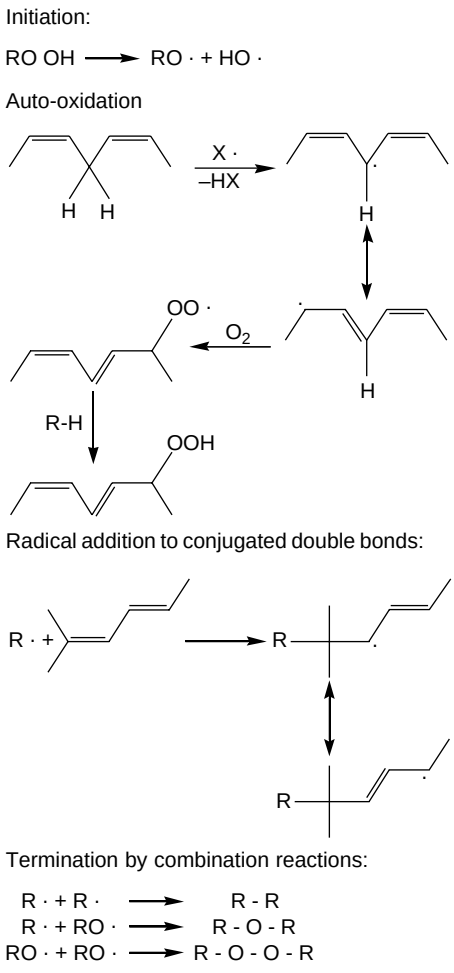

Fig. 1. Schematics of the oxidative drying of oils used in alkyd coatings [5].

A direct way of monitoring the cross-linking reaction is given e.g. by measuring the changes in IR absorption [18–21]. One of the drawbacks of this approach is that the specific absorption bands overlap with other bands in the spectrum, which renders quantitative data analysis difficult. The other major drawback is that information is not provided as a function of spatial (i.e. in depth) position. Raman spectroscopy has already been used to investigate the chemical cross-linking mechanism of alkyd coatings in bulk films [22,23]. Confocal Raman microspectroscopy has shown its efficiency for depth profiling of coatings, composites and laminates [24–28]. Raman microscopy offers a good combination of spatial resolution and chemical characterization. The confocal aperture is designed to collect the Raman scattering only from a distinct laser focal sampling volume within the diffraction limit [29]. Thus, the Raman signal from a small volume element in the sample can be selected and separated from the signals originating from the surrounding material, provided that there are no optical aberrations that degrade the depth resolution.

We used CRM in this study to investigate the cross-linking mechanism in alkyd coatings across the film thickness. This technique can potentially measure the onset of cross-linking spatially resolved in alkyd films [17,30]. During cross-linking, the concentration of double bonds in alkyd coatings decreases and finally approaches zero. Monitoring the change in the spatial distribution of C=C double bonds in the coating layer (as a function of depth) gives information on the progress of the drying process. It is important to note at this juncture that there is no direct relationship between the double bond concentration and the extent of cross-linking. Following full double bond consumption the cross-linking process can still continue. In addition, other effective cross-linking sites (chemical and physical) can contribute to the value of the elastically effective network cross-link density, which determines mechanical performance.

Any quantitative description of the film formation process must take into account that the mechanical response of the polymer changes as a function of time in a crosslinked

polymer. Since the cross-linking process is initiated at the surface, a so-called cross-linked 'skin' layer can form at the surface. In order to assure the progress of the network formation, a certain amount of oxygen must pass through this layer, which is less permeable to the oxygen, to reach the film interior [31]. During the cross-linking, with increasing cross-link density and decreasing unsaturation at a given depth, the mobility of the molecules decreases. This limits the oxygen diffusion through the already dried layer [32]. Oxygen solubility in the cross-linking film is also assumed to decrease. As a result of the gradient in oxygen permeability (combined effect of solubility and diffusion), and related also to the variation of C=C concentration vs. depth, alkyd films dry heterogeneously. In this work, the extent and rate of crosslinking as a function of drying time and depth in alkyd coatings will be discussed, and the influence of oil length, thickener, and solvent on the drying front will be elucidated.

2. Experimental

2.1. Materials

Water-borne (WB) alkyd emulsions, as well as solvent-borne (SB) alkyds (alkyd resin dissolved in 1-methoxy-2-hydroxypropane) were studied. Alkyd resins (supplied by Akzo Nobel B.V.) based on sunflower fatty acids with oil lengths of 40% (OL40), 55% (OL55) and 75% (OL75), respectively, were used as binders. The term oil length is related to the fatty acid content of the alkyd resin with respect to the total weight of corresponding solvent-free solids. A water-soluble cobalt salt ($Co(NO_3)_2 \cdot 6H_2O$) drier was added to the alkyd emulsions and another cobalt containing formulation was added to the solvent-borne alkyds to catalyze the cross-linking process [33]. The quantity of the cobalt drier was 0.1 wt% of cobalt on the solid resin weight for both the solvent-borne and water-borne alkyds, respectively. An associative thickener was used to adjust the viscosity of the alkyd emulsion coatings at 4 wt% of the solid resin. The thickener was a hydrophobically modified polyurethane compound. The alkyd films were cast on glass plates using a 150 μm applicator, and then the coating films were dried under normal laboratory conditions.

2.2. Techniques

CRM was used to measure the double bond concentration decrease during the chemical cross-linking process. Raman spectra of the alkyd films were recorded by a custom-made confocal Raman microspectrometer using a 25 μm confocal pinhole [29]. A Kr ion-laser (Coherent, Innova 90-K) provided the excitation wavelength of 647.1 nm. A dry 63X objective (Zeiss Plan Neofluar) with a numerical aperture (NA) of 0.85 was used for the acquisition of all Raman spectra. The spectra were recorded with 30 mW laser power, and accumulation times of 30 s were employed. A confocal set-up (Fig. 2) ensured the optical sectioning in the depth of the film. The depth profiling experiment was started by taking a spectrum at the surface of the film, followed by collecting spectra at steps

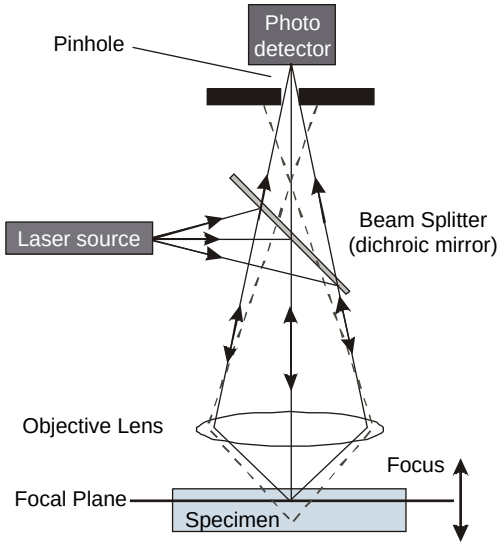

Fig. 2. Confocal Raman microspectroscopy experimental set-up. The broken line labels the out of focus laser light beam, which cannot reach the detector.

of 4 μm in depth until the glass substrate was reached. The scattering efficiency of the C=C bond peak at 1655 cm^{-1} was extracted and normalized to a reference peak at 1000 cm^{-1}, which was unaffected by curing. CRM can be used for quantitative analysis since the Raman signal is proportional to the concentration of the given Raman-active group absorbing at the chosen wavelength. The steps of the spectral corrections will be described in detail in the 'results' section.

In our experiments we collected spectra of focal volumes, which were located deeper in the film than the nominal depth [34,35]. The size of the sampled volume increases as the focus point goes deeper into the sample. Difficulties in data evaluation arise from the diffraction and the refraction limitations of the measurement. The refraction influences the depth resolution and spatial accuracy of confocal Raman microspectroscopy. To correct for these deviations a method was established for determining the true point of focus and depth of focus as a function of the apparent focal depth [34]. A short summary of this correction method can be found in the Appendix A. The factors affecting the depth of resolution are the optical properties of the sample, the numerical aperture of the microscope objective, and the magnifying power of the objective lens.

3. Results and discussion

The onset of the cross-linking was monitored by measuring the disappearance of the *cis* C=C stretching band at 1655 cm^{-1} (Fig. 3) using CRM. The aliphatic *cis* C=C stretching vibration gives rise to strong Raman scattering, and can be clearly differentiated from the carbonyl band at 1729 cm^{-1} and the characteristic doublet band due to the aromatic C=C stretches around 1600 cm^{-1}. A widening and shifting of the C=C band was observed with the advancement of cross-linking due to the double bond isomerization from *cis* to *trans* (a shoulder appears at 1670 cm^{-1}) and accompanying

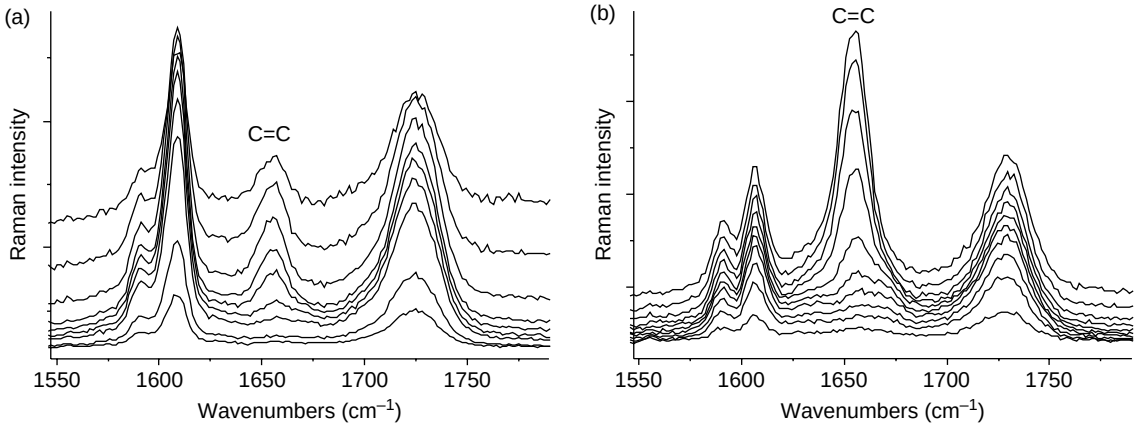

Fig. 3. Raman microscopy spectra as a function of depth in (a) OL40 and (b) OL75 alkyd coatings. The individual spectra from bottom to top represent optical sections as a function of increasing depth from the surface.

formation of conjugated structures (at 1630 cm^{-1}) [18]. FTIR showed evidence of the above-mentioned double bond rearrangements [18]. The decrease of the antisymmetric stretching of *cis* C=C at 3012 cm^{-1} could also be followed by Raman spectroscopy [18]. However, in case of our samples more vibration bands overlap with each other in this spectral region, which makes the quantitative determination of C=C bond concentration difficult to perform.

3.1. Network formation in alkyds

The CRM measurements reveal the decay of double bond concentration as a function of film nominal depth for specimens, which were dried for different times. Fig. 4(a) shows a typical example of the cross-sectional intensity data, where the C=C Raman intensity vs. nominal depth for OL55WB samples dried for different times is depicted. The Raman intensity was calculated as the integrated area under the peak used. The individual lines from top to bottom represent graphs belonging to samples dried for increasing times involving 3, 8 h, 1 day, 2 days, 3 days, 5 days and 6 days, respectively. In Fig. 4(a) the top gray line corresponds to results at zero drying time. Nominal depth is defined as the distance between the preset focal point within the film and the film surface. The curve at the top ($t=0$ h) was measured on a sample from which the solvent was removed and the chemical drying was blocked. Prior to the measurement this sample was kept under nitrogen to assure that the oxidation is prevented, i.e. that all the C=C bonds remained. It is assumed that the C=C concentration is homogeneously distributed in the alkyd coatings before the onset of the chemical oxidation. However, even in the unreacted samples, the measured intensity profiles show 'apparent' differences in the C=C peak areas (Fig. 4(a)) as a function of depth. This intensity variation is due to the effects related to the increase of the sampling volume as described in the Appendix A. It can be seen in the graphs that with increasing drying time the overall C=C concentration decreases. However, because the sampling volume changes as a function of the measuring depth, it is difficult to draw conclusions from Fig. 4(a) for the 'true' C=C consumption as a function of depth. The distorting effect of changes in sampling volume with increasing nominal depth and the variation of the C=C concentration must be adequately considered.

As a first approach to correct for the increasing sample volume with increasing nominal depth the area of the C=C bond peak at 1655 cm^{-1} was normalized to the band area of the aromatic group (at 1004 cm^{-1}), which is unaffected by curing, thus will have a constant intensity across the film. By using the ratio of the two Raman intensities, the influence of the increasing sampling volume is excluded. This bond is effectively used as an internal standard. Possible effects, such as laser intensity fluctuations and other time-dependent optical changes are eliminated by dividing the area of the C=C peak by the peak area of the internal standard. The resulting normalized curves are shown in Fig. 4(b) for

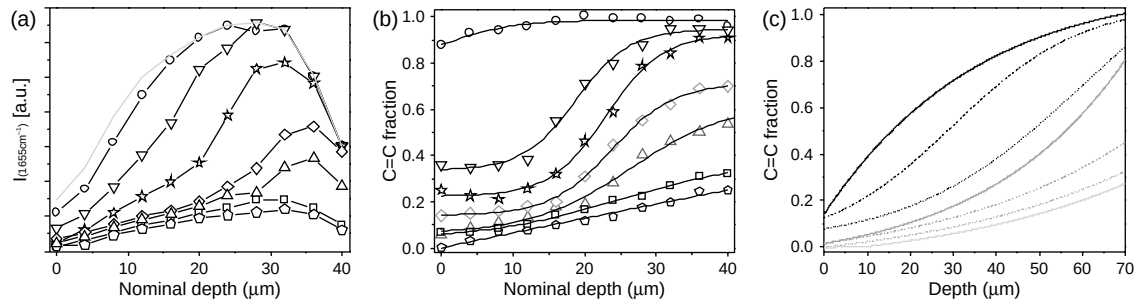

Fig. 4. (a) Measured C=C bond intensity vs. nominal depth, (b) normalized C=C fraction decay vs. nominal depth, (c) C=C fraction decay vs. corrected depth as a function of drying times for OL55WB. The individual lines from top to bottom represent graphs belonging to samples dried for increasing times including 3, 8 h, 1 day, 2 days, 3 days, 5 days, and 6 days, respectively.

OL55WB. These curves show the C=C fraction vs. nominal depth as a function of drying times. Every calculated point stands for an average C=C fraction in the actual focal volume, which is more extended and placed progressively deeper in the film than the nominal values (the correction for the depth is discussed in the Appendix A).

To determine the concentration profiles as a function of the corrected real ('true') depth, the measured Raman intensity

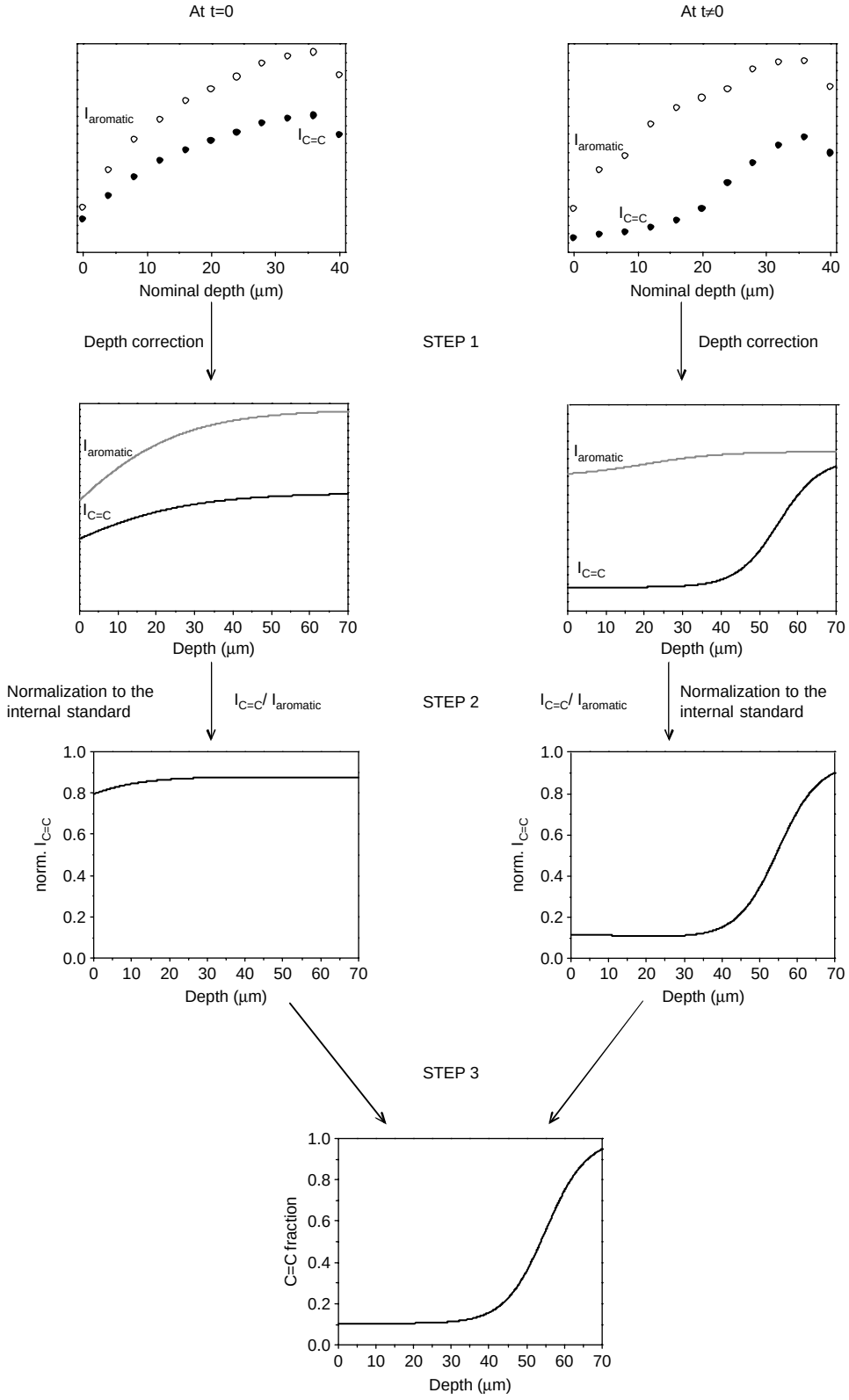

Fig. 5. Scheme for the numerical procedure to determine the C=C bond fractional concentration as a function of the 'true' depth.

C=C vs. nominal depth curves shown in Fig. 4(a) must be corrected for the increasing sample volume and film depth as shown in Fig. 5. In the first step (see STEP 1 in Fig. 5) the Raman intensity of C=C bonds, $I_{C=C}$, as a function of nominal depth was corrected for the increasing sampling volume and depth of focus according to the method described in Appendix A. This depth correction was also carried out with the Raman intensity of the aromatic groups within the film, $I_{aromatic}$, vs. nominal depth curves (internal standard). Then in the second step (see STEP 2 in Fig. 5) the depth corrected Raman intensities of C=C bonds were normalized to the depth corrected Raman intensity of the internal standard by dividing $I_{C=C}$ with $I_{aromatic}$ (aromatic compound) at every depth value resulting in a normalized C=C intensity, $I_{C=C}$, as a function of depth. This procedure was performed for all $I_{C=C}$ at various drying times, including $t=0$. Then all normalized $I_{C=C}$ intensity values vs. depth at $t\neq 0$ were divided by the normalized $I_{C=C}$ vs. depth at $t=0$ resulting in a C=C fraction (see STEP 3 in Fig. 5). Based on these calculations, the C=C double bond fraction as a function of the 'true' corrected film depth is obtained as final normalized C=C concentration profile. Results obtained as a function of depth after several drying times are shown in Fig. 4(c) as an example.

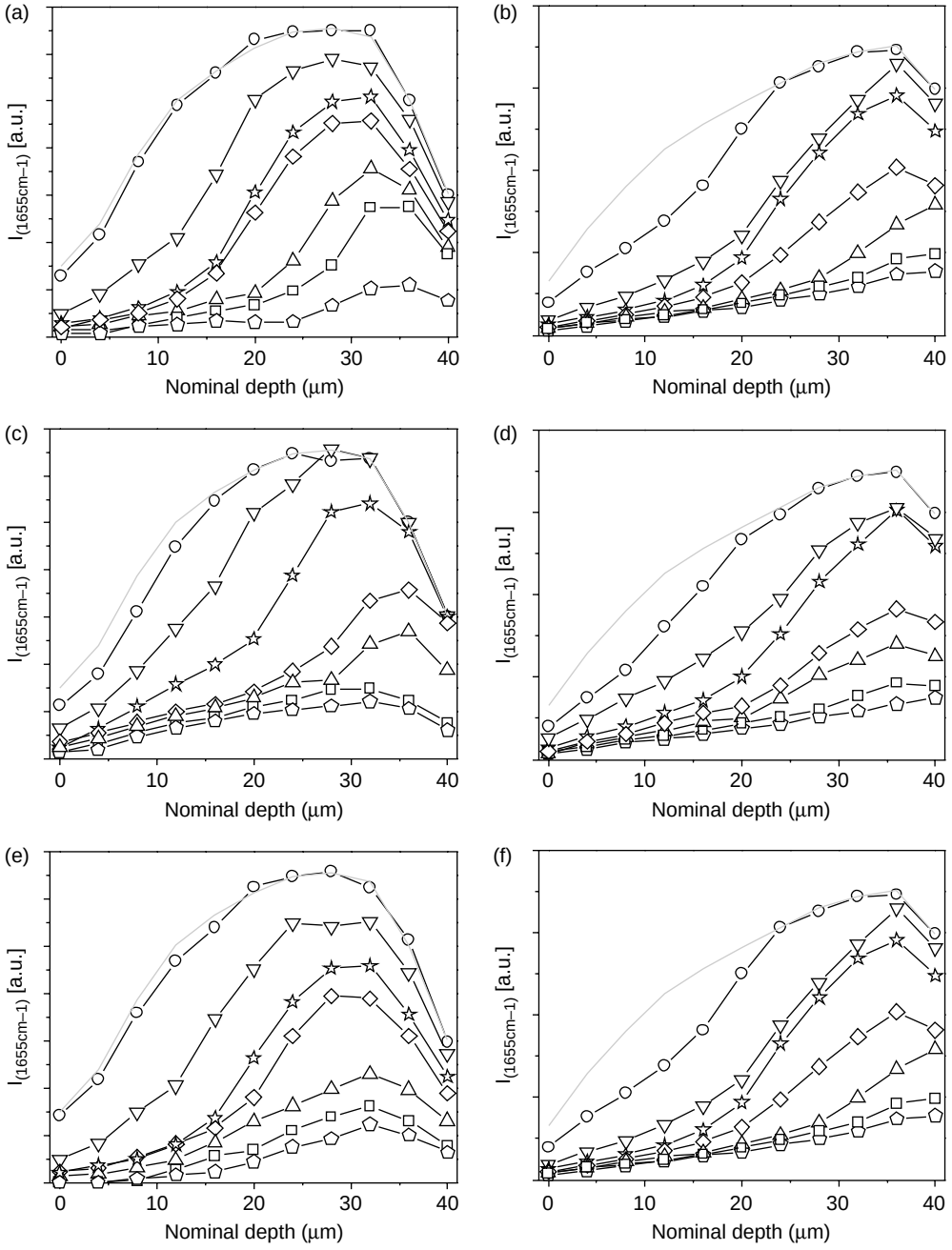

Fig. 6. Measured C=C bond intensity vs. nominal depth as a function of drying times in samples of (a) OL40WB, (b) OL75WB, (c) OL40SB, (d) OL75SB, (e) OL40WBt (f), OL75WBt. The individual lines from top to bottom represent graphs belonging to samples dried for increasing times including 3, 8 h, 1 day, 2 days, 3 days, 5 days, and 6 days, respectively.

Further results for other samples are also shown in Fig. 6(a)–(f) displaying the Raman intensity of C=C double bonds as a function of nominal depth. In Fig. 7(a)–(f) the C=C bond fraction as a function of the real depth after 3, 8 h, 1 day, 2 days, 3 days, 5 days and 6 days of drying, respectively, are depicted.

The extent of cross-linking is not homogeneous in depth, as can be observed from the measured and calculated profiles. The double bond consumption and corresponding chemical cross-linking proceeded from the surface (in direct contact with air) in the direction of the substrate. From the sample surface up to a depth of 20 μm there is no significant difference in C=C fraction as a function of film depth. The drying is homogeneous in the top surface layer of the film. At higher depths, a gradient in the C=C fraction is observable, showing an increase of the C=C fraction with increasing depth in the film.

In the course of the depth correction calculations it was assumed that the resulting C=C fraction vs. depth curves can be approximated by a Boltzmann function (Eq. (A7) in Appendix A). The corresponding sigmoidal curves can be divided into three regions, including two plateau levels and a transition region in between. In the lower plateau level which is situated close to the surface, the C=C consumption is homogeneous. The higher plateau level is only visible after

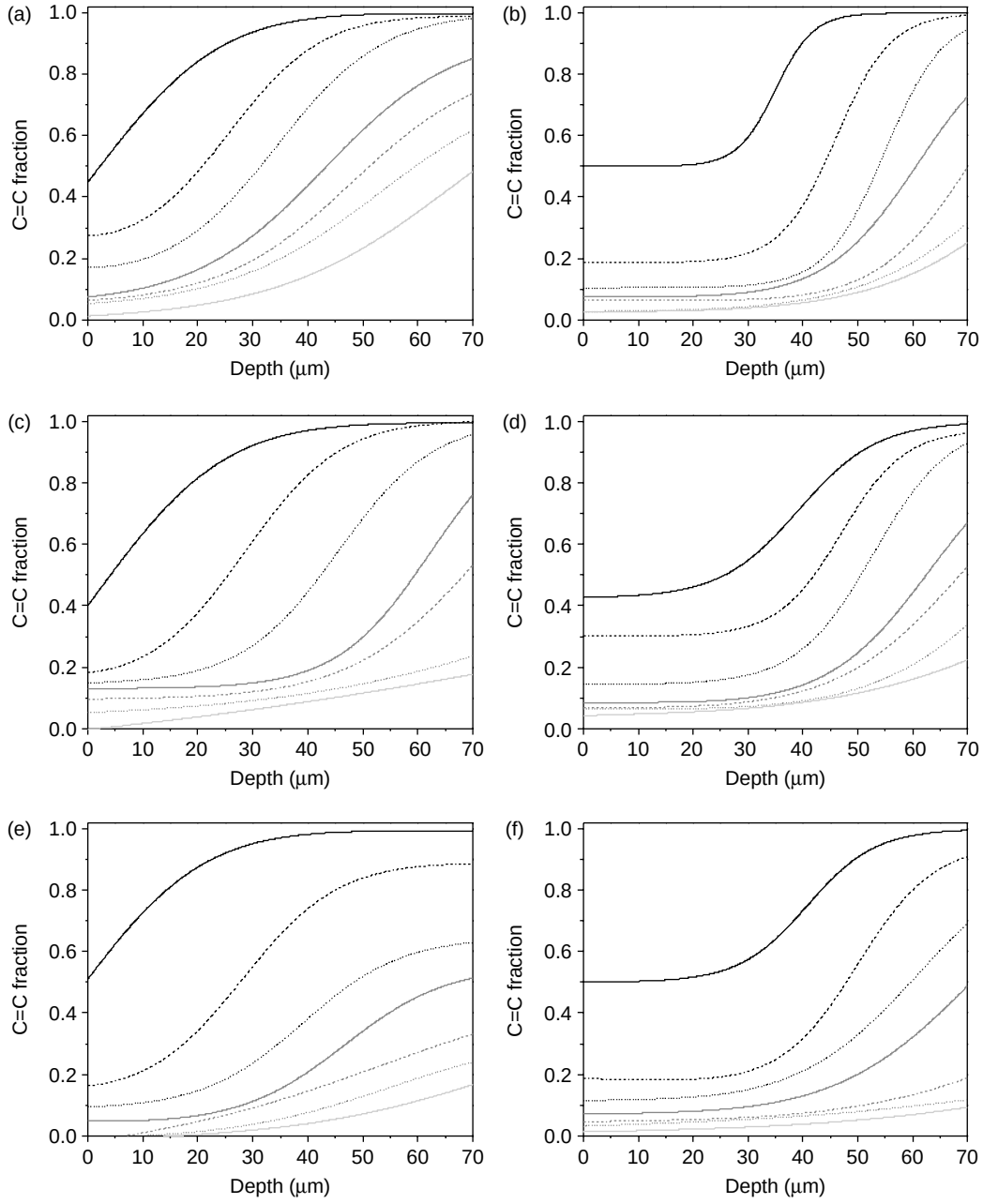

Fig. 7. C=C fraction decay vs. corrected depth as a function of drying times in samples of: (a) OL40WB, (b) OL75WB, (c) OL40SB, (d) OL75SB, (e) OL40WBt, OL75WBt. The drying times from top to bottom are 3, 8 h, 1 day, 2 days, 3 days, 5 days and 6 days, respectively. The results include water borne (WB) and solvent borne (SB) specimens, without and with thickener (WBt). The number following the label 'OL' refers to the oil length.

short drying times. After longer drying times this second plateau disappears. The transition region became wider during the course of drying and its center moved towards deeper layers of the films with increasing curing time. The center of the transition region provides information on the progress of cross-linking. The transition region of the Boltzmann curve fitted can be considered as an apparent 'drying front'. The movement of the apparent 'drying front' can be observed in Fig. 7.

The 'drying front' suggests a limiting factor in the cross-linking process, which is presumed to be related to the limited penetration of oxygen into the coating. Based on the measured data, the film forming profiles are assumed to be the result of interplay among oxygen penetration and diffusion, and double bond concentration. In the outer layer the C=C consumption is homogeneous. From this it can be concluded that there is no diffusion limitation here and the oxidation reaction is the rate-determining step. Beyond a certain film thickness the oxygen diffusion (mass transport) becomes the limiting process. A full model describing details of a mechanism proposed will be published in a subsequent paper.

3.1.1. Influence of oil length

The drying behaviour of alkyds with different oil length values was also compared. The oil length is an important parameter of alkyds since the absolute amount of double bonds in the alkyd coatings increases with increasing oil length. The double bond fraction as a function of the corrected depth for alkyds of different oil length is shown in Fig. 7(a: OL40, b: OL75). Different trends were measured for the alkyds of different oil lengths. After 3 h drying for OL40 and OL55, the decay of C=C bonds just started. For OL75 close to the surface approximately 50% of the C=C bonds disappeared after three hours of atmospheric exposure. The decay of double bond concentration is apparently slower for OL40 than for OL75. A particularly large difference is observable in the deeper regions of the coating films after 5 and 6 days of drying, respectively. The OL55 sample behaved similar to the OL40 sample. The results indicate a stronger effect of the diffusion limitation during the drying of OL40 and OL55 compared to the OL75. The higher viscosity of OL40 samples can explain the larger oxygen diffusion limitation. The movement of the 'drying front' as a function of oil length in Fig. 8 also clearly shows the difference in the cross-linking behaviour among the alkyds of different oil length. After certain drying times the position of the transition region is situated deeper in OL75 samples than in OL40 and OL55.

3.1.2. Influence of the thickener

In subsequent experiments a thickener was mixed into the alkyd emulsion. A thickener is very often added to alkyds to modify the rheological properties of the coatings [4,5]. Fig. 7(e) and (f) show the drying profiles of coating samples with thickener. The thickener seems to have an accelerating effect on the chemical oxidation, especially in the deeper layers of the coating films. Fig. 9 shows also a noticeable effect of thickener on the movement of the 'drying front'. This accelerating effect is less pronounced in case of long oil

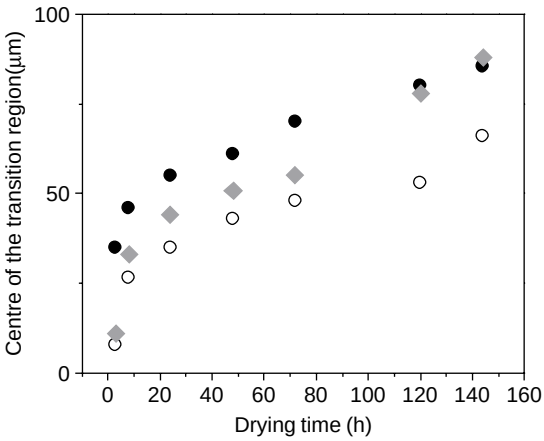

Fig. 8. Advancement of the drying front as a function of oil length: OL40WB (○), OL55WB ◆ and OL75WB (●).

alkyds, since the crosslinking reaction was already faster without modifier. It seems that in the presence of the thickener a more homogeneous and faster drying takes place. It is known that thickeners plasticise coatings, thus they may increase oxygen mobility in the coating film, resulting in faster kinetics. This reasoning can explain also the stronger effect for OL40 since the short oil resin has a much higher viscosity at room temperature than OL75.

3.1.3. Influence of the solvent

The drying behaviour of alkyd emulsion coatings and solvent-borne alkyds was also compared. The drying profiles for solvent-borne alkyds are displayed in Fig. 7(c) and (d) as a function of corrected depth. If solvent-borne OL40 alkyd was used, faster kinetics was observed than for water-borne alkyds. There is a faster reaction in the first few hours and the decay of C=C concentration in the deeper layers was also much faster for the solvent-borne specimens. Furthermore, the comparison of the advancement of the 'drying front' between the solvent-borne and water-borne OL40 alkyds shown in Fig. 9 underlines the previous statements. Oxygen is usually considered more soluble in a less polar organic solvent than in water [37]. In addition, for solvent-borne alkyds around 5% of the organic

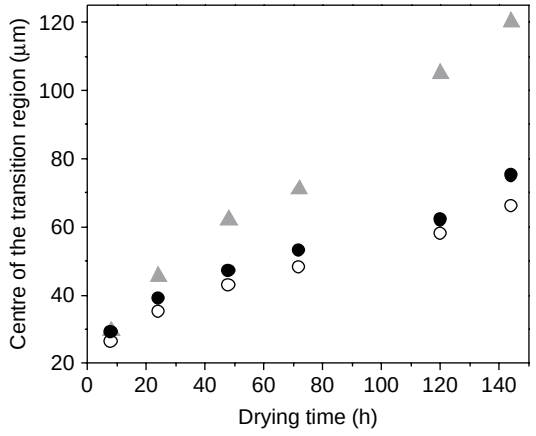

Fig. 9. Advancement of the drying front for OL40WB (○), OL40WB with thickener added (●) and OL40SB ▲ coatings.

solvent remains in the coating film, while all the water evaporates within 1 h after application of the coating. The remaining solvent reduces the viscosity of the coating, and decreases the glass transition temperature. Thus the oxygen mobility is higher in the drying solvent-borne alkyd films, which can explain the observed behaviour. In case of OL75 the influence of the solvent is negligible. This can be (qualitatively) due to the fact that OL75 alkyd even without any solvent has a low viscosity, thus adding organic solvents does not cause a significant change in the mobility of oxygen.

4. Conclusions

Confocal Raman microspectroscopy was successfully applied to investigate the oxidative cross-linking as a function of film depth in drying alkyd coatings. This type of information concerning the cure profile helps to understand the buildup of stress in the drying film. This technique provides new insights into the network formation of alkyds. In addition, the results were obtained in a non-invasive fashion. The method described here can potentially measure C=C consumption, which is related to the onset of cross-linking, spatially resolved in alkyd films. Based on the results it is clear that the chemical cross-linking is not homogeneous in the depth of the coating. Different drying profiles were obtained for the long and short oil alkyd films, respectively. The consumption of C=C bonds is slower in the deeper layers of the alkyd films for the short oil length alkyds. Adding thickener to the coating and changing the water into organic solvent has a similar influence on the drying process: both plasticize the coating film, thus accelerate the chemical drying process. Based on the measured concentration profiles across the film thickness the 'true' concentration profiles were calculated. The shape of the drying profiles suggests that there is oxygen penetration control over the cross-linking process. The cross-link density profiles (related to double bond depth profiles) can be described by models assuming concentration changes in films during chemical reactions with gasses, accompanied by mass transfer of gas molecules.

Acknowledgements

This work was supported by the Priority Program Materials (PPM) of the Netherlands Foundation for Chemical Research (NWO-CW) and the Dutch Polymer Institute (DPI). Akzo Nobel is acknowledged for providing alkyd samples. The authors thank Prof. Brenny van Groesen for the many helpful discussions.

Appendix A

A.1. Calculation of the depth correction in CRM

The confocal aperture is designed to collect the Raman scattering from a distinct laser focal volume. However, in practice the extent of the volume from which light is collected is determined also by refractive index mismatch. Consequently, we collected spectra of focal volumes, which are positioned deeper in the film than the nominal depth, and this volume increases as the focus point goes deeper into the sample [34,35]. This occurs because the laser intensity spreads over a larger sample volume due to diffraction and the refraction limitations of the measurement and the set value of the film depth must be corrected to obtain true depth values. The factors affecting the depth resolution include the optical properties of the sample, the numerical aperture of the microscope objective, and the magnifying power of the objective lens [36].

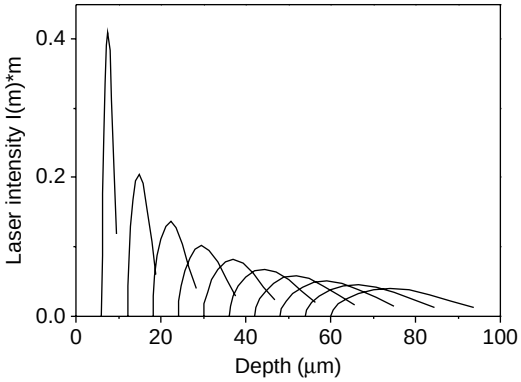

Fig. A1. Laser intensity, $mI(m)$ vs. focal position. The curves from left to right are standing for nominal depth intervals of 4 μm at consecutive depth increments.

To correct for these deviations a method was established determining the true point of focus and depth of focus as a function of the apparent focal point [34]. In this analysis, the effect of diffraction is neglected and only the influence of the refraction was considered. Based on the work of Everall [34], the laser intensity distribution was calculated as a function of focal position in the film (Fig. A1).

The true focal position is given by the following equation:

$$z(m) = x\left[m^2\frac{\mathrm{NA}^2(n^2-1)}{(1-\mathrm{NA}^2)} + n^2\right]^{1/2} \tag{A1}$$

In this equation x is the nominal depth, m is the normalized radius of the aperture, NA is the numerical aperture and n is the relative refractive index of the sample. Based on Eq. (A1) the range of laser focal positions within the sample, called the depth of focus (dof), is given by $z(m=1)-z(m=0)$:

$$\mathrm{dof} = x\left[\left[\frac{\mathrm{NA}^2(n^2-1)}{(1-\mathrm{NA}^2)} + n^2\right]^{1/2} - n\right] \tag{A2}$$

This equation shows that not only the point of focus but also the depth of focus increases linearly with x.

The intensity distribution, I, can be expressed in terms of the normalized radius of aperture, m:

$$I(m) = I_0 \mathrm{e}^{-2m^2/\varphi^2} \tag{A3}$$

where φ stands for fill factor. If the radial intensity distribution of the laser beam is $I(m)$, then the overall intensity of all rays originating from within the radius m is proportional to $mI(m)$, assuming circular symmetry. Thus we must weigh the

contribution of each ray by the value of m. Fig. A1 shows the laser intensity, $mI(m)$ vs. true depth. The curves from left to right are standing for nominal depth intervals of 4 μm at consecutive depth increments.

Raman scattering can occur at any point within the illuminated regions, but the probability of a Raman photon passing through the confocal aperture to reach the detector will depend on the point of origin. We must estimate the relative contributions of Raman scatter from each point as a function of depth. There are two methods for weighting the Raman response, $R(z)$ according to the following formulas [34]:

$$R(z) = m^2 I(m) \tag{A4}$$

$$R(z) = mI(m)\left(\mathrm{NA}_{\mathrm{eff}}^2\right) \tag{A5}$$

The confocal weighting method (Eq. (A4)) assumes that the numerical aperture works perfectly and only photons scattered with a specific angle will pass through the confocal aperture. The second approach (Eq. (A5)) simply weights every point by multiplication using the square of the effective numerical aperture. These two Raman response profiles are very similar and both can give a reasonable fit to the experimental data [34]. In our case the confocal weighting method was applied. The response function measured, $c(x)$, is the convolution of the Raman response distribution $R(z,x)$ with the real concentration profile, $C(z)$, of the sample:

$$c(x) = \int_0^T C(z)R(z,x)\mathrm{d}z \tag{A6}$$

The normalized concentration profiles can be fitted by a suitable function. We chose the Boltzmann equation as this function exhibits a saturation plateau and a transition region (sigmoidal shape). We assumed that the real concentration profile as a function of depth could also be fit to the Boltzmann equation:

$$C(z) = \frac{A_1 - A_2}{1 + \mathrm{e}^{(z-z_0)/w}} + A_2 \tag{A7}$$

where A_1 and A_2 are the plateau concentrations, z_0 is the center of the curve and w is the width of the sigmoidal curves.

For every measured point the following equations can be written:

$$c_4 - \int_{z_{m=0}}^{z_{m=1}} C(z)R_4(z,x)\mathrm{d}z = D_4 \tag{A8}$$

$$c_8 - \int_{z_{m=0}}^{z_{m=1}} C(z)R_8(z,x)\mathrm{d}z = D_8$$

$$c_i - \int_{z_{m=0}}^{z_{m=1}} C(z)R_i(z,x)\mathrm{d}z = D_i$$

where c_x and $R_x(z,x)$ are the measured concentrations and Raman intensity, respectively, at $x = i$ [μm] nominal depth. In the course of the calculations, the differences, D_x, described in the above written set of equations are minimized, resulting in numerical values of the unknown parameters (A_1, A_2, z_0 and $\mathrm{d}z$) of the real concentration profiles, $C(z)$.

References

[1] Hek Hd, Zabel KH, Geurink PJA. Surf Coat Aust 1998;35:14–22.
[2] Hofland A. In: Glass JE, editor. Technology for waterborne coatings, vol. 663. Washington, DC: ACS; 1997. p. 183–95.
[3] Beetsma J. Pigm Res Technol 1998;27:12–19.
[4] Prideaux J. Surf Coat Int 1993;76:177–83.
[5] Wicks ZW. Organic coatings. New York: Wiley; 1999.
[6] Lanson HJ. In: Mark HF, Bikales NM, Overbergen CG, Menges G, editors. Encyclopedia of polymer science and engineering, vol. 1. New York: Wiley; 1985.
[7] Paul S. Surface coatings. New York: Wiley; 1985.
[8] Muizebelt WJ, Hubert JC, Venderbosch RAM, Lansbergen AJ, Klaasen RP, Zabel KH. J Coating Technol 1998;70:53–9.
[9] Swern DJ, Coleman JE, Knight HB, Ricciuti C, Willits CO, Eddy CR. J Am Chem Soc 1953;75:3135–7.
[10] Muizebelt WJ, Hubert JC, Venderbosch RAM. Progr Org Coat 1994;24:263–79.
[11] Muizebelt WJ, Nielen MWF. J Mass Spectrom 1996;31:545–54.
[12] Kumarathasan R, Rajkumar AB, Hunter NR, Gesser HD. Progr Lipid Res 1992;31:109–26.
[13] Oyman ZO. Prog Org Coat 2003;48:80–91.
[14] Glover PM, Aptaker PS, Bowler JR, Ciampi E, McDonald PJ. J Magn Res 1999;139:90–7.
[15] Wallin M, Glover PM, Hellgren A-C, Keddie JL, McDonald PJ. Macromolecules 2000;33:8443–52.
[16] Comte C, Stebut Jv. Surf Coat Technol 2002;154:42–8.
[17] Mirone G, Marton B, Vancso GJ. Eur Polym J 2004;40:549–60.
[18] Ellis G, Claybourn M, Richards SE. Spectrochim Acta 1990;46A:227–41.
[19] Hartshorn JH. J Coating Technol 1982;54:53.
[20] Salazar-Rojas EM, Urban MW. Prog Org Coat 1989;16:371–86.
[21] Mertzel E, Koening JL. Adv Polym Sci 1986;75:73–85.
[22] Claybourn M, Agbenyega JK, Hendra PJ, Ellis G. Adv Chem Ser 1993;236:443–82.
[23] Agbenyega JK, Claybourn M, Ellis G. Spectrochim Acta 1991;47A:1375–88.
[24] Sammon C, Hajatdoost S, Eaton P, Mura C, Yarwood J. Macromol Symp 1999;141:247–62.
[25] Belaroui F, Grohens Y, Boyer H, Holl Y. Polymer 2000;41:7641–5.
[26] Tabaksblat R, Meier RJ, Kip BJ. Appl Spectrosc 1992;46:60–8.
[27] Schrof W, Beck E, Koniger R, Reich W, Schwalm R. Prog Org Coat 1999;35:197–204.
[28] Schrof W, Beck E, Etzrodt G, Hintze-Bruning H, Meisenburg U, Schwalm R, et al. Progr Org Coat 2001;43:1–9.
[29] Sijtsema NM, Wouters SD, Grauw CJd, Otto C, Greve J. Appl Spectrosc 1998;52:348–55.
[30] Marton B, Ven LGJvd, Otto C, Uzunbajakava N, Hempenius MA, Vancso GJ. ACS Polym Mater Sci Eng 2003;88:445–6.
[31] Zetterlund PB, Johnson AF. Polymer 2002;43:2039–48.
[32] Crank J, Park GS. Diffusion in polymers. New York: Academic Press; 1968.
[33] Östberg G, Huldén M, Bergensthahl B, Holmberg K. Prog Org Coat 1994;24:281–97.
[34] Everall NJ. Appl Spectrosc 2000;54:773–82.
[35] Everall NJ. Appl Spectrosc 2000;54:1515–20.
[36] Claybourn M, Luget A, Williams KPJ. Multidimensional spectroscopy of polymers. vol. 598. Washington, DC: ACS; 1995 p. 41–60.
[37] Dean JA, editor. Lange's handbook of chemistry. New York: McGraw-Hill; 1999.